Self-Diffusion of a Rodlike Virus in the Isotropic Phase†

Randall C. Cush and Paul S. Russo*

Department of Chemistry and Macromolecular Studies Group, Louisiana State University, Baton Rouge, Louisiana 70803

Received April 5, 2002
Revised Manuscript Received August 20, 2002

Introduction. Dynamics in concentrated solutions and melts is a recurring theme in polymer research.[1,2] While much progress has been made in random coil systems and branched polymers, only limited experimental data[3,4−10] are available to test theories proposed for concentrated or semidilute solutions of rods.[11−20] Such theoretical treatments began with the work of Doi and Edwards[11,12] which supposes the onset of entanglement to occur at a number density $\nu = 1/L^3$, where L is the rod length. Without affecting longitudinal translation, topological constraints dispossess the rods of lateral motion, causing D_{self} to fall by half. This reduction should be nearly complete once the number density has reached $\nu = 1/dL^2$, where d is the rod diameter. According to Onsager,[21] a transition to a liquid crystalline phase occurs near $\nu^* = 16/\pi dL^2 \cong 5/dL^2$. An optical tracer self-diffusion study[3] of the stiff, helical homopolypeptide, PBLG (poly(γ-benzyl-α-L-glutamate)), revealed that D_{self} was a weak function of concentration until the condition $\nu dL^2 = 0.5-1$ was met. Beyond this concentration, the authors observed a downturn in D_{self} for a range of molecular weights. The regime in which D_{self} varied only weakly with concentration was not observed for very rigid colloidal boehmite particles, and it was suggested that the flexibility of PBLG underlies this difference.[4,5] Only additional data on rigid and nearly rigid systems can resolve the issue. In the very rigid limit, nature provides an excellent model system in the form of tobacco mosaic virus (TMV). This paper describes the use of fluorescence photobleaching recovery (FPR) to follow the optical tracer self-diffusion of TMV throughout the isotropic regime.

Materials and Methods. TMV was purified from infected plant leaves by a differential centrifugation method described previously.[22] Purified virus and labeled virus were characterized by dynamic light scattering (DLS) and analytical ultracentrifugation. TMV was labeled with the 5-isomer of fluorescein dichlorotriazine or 5-DTAF (Molecular Probes). Briefly, 20 μL of 1 M sodium bicarbonate buffer at pH = 9.0 was added to 200 μL of a stirred TMV solution at 20 mg/mL in 0.01 M sodium phosphate buffer at pH = 7.4 with 0.003 M sodium azide. To this DTAF in DMSO at 10 mg/mL was immediately added, and the reaction was allowed to run for about 1 h. A molar excess of 800 (relative to the number of TMV particles) of DTAF was used. The dye can react with amine and thiol groups on protein residues in alkaline solution and possibly to terminal hydroxyl groups if these better nucleophiles are not accessible.[23] Labeled TMV was separated from free dye by gel filtration using Sephadex G-25 (Sigma). It is estimated from spectrophotometric measurements that the labeling ratio was 130 dyes per TMV particle, using a molar extinction coefficient of 82 000 M^{-1} cm^{-1} at 4920 Å for DTAF.[23] This amounts to only about 0.2% increase in the molar mass of the TMV. Samples for FPR were made by mixing labeled TMV (L-TMV) with unlabeled TMV to give a final concentration of 0.5 mg/mL L-TMV in all samples at or above 0.5 mg/mL total TMV concentration. Samples at lower concentrations were made by diluting the 0.5 mg/mL L-TMV with buffer. All samples were prepared in 0.01 M sodium phosphate buffer at pH = 7.4 with 0.003 M sodium azide to prevent growth of microbes. Samples were loaded into rectangular capillary tubes with a path length of 100 μm (Vitrocom) and stored at 4 °C when not in use.

The FPR instrument was similar to that described earlier[3] with modifications to improve signal quality and data analysis.[24] The device is built around an Olympus BH2 epifluorescence microscope. An argon ion laser casts a striped pattern onto the sample by illuminating a Ronchi ruling in the rear image plane of the microscope. A brief, intense bleaching pulse destroys about 10% of the dye molecules, after which the laser intensity is reduced by a factor of about 2000. Two opposing loudspeakers driven by a 5 W amplifier fed by a triangle wave cause the Ronchi ruling to oscillate a distance equal to the width of one stripe. The resulting signal modulation makes it easier to detect shallow photobleaches, among other advantages.[25] The peak-to-peak amplitude, representing contrast, is measured by a triggered peak voltage detector. Diffusion causes the contrast to decay with time, t, according to

$$C(t) = C(0)e^{-\gamma t} \tag{1}$$

The decay rate, γ, is DK^2, where D is the translational diffusion coefficient and K is the spatial frequency,

$$K = 2\pi/l \tag{2}$$

where l is the period of the striped pattern in the sample, determined by the Ronchi ruling and objective lens. The sample temperature was maintained at 25 ± 0.02 °C with a recirculating bath, connected to a sample holder on the microscope stage.

The DLS instrument used to characterize the TMV has been described elsewhere,[22] except that a Coherent Innova 90-6 laser producing up to 900 mW at 5145 Å provided the incident beam. For L-TMV samples, a He−Ne laser producing up to 20 mW at 6328 Å, far from the absorption peak for DTAF, was used to avoid effects due to absorbance. From depolarized DLS experiments, one can simultaneously measure the translational and rotational diffusion coefficients, D_{trans} and D_{rot}, respectively.[22] Analytical ultracentrifugation to determine the sedimentation coefficient was performed on a Beckman XL-A analytical ultracentrifuge equipped with absorption optics.

Results and Discussion. When corrected for temperature and viscosity, the translational and rotational diffusion coefficients of the TMV, $D_{t,20w} = (4.5 \pm 0.3) \times 10^{-8}$ cm^2 s^{-1} and $D_{r,20} = 278 \pm 10$ s^{-1}, agreed with literature values, which are discussed critically in ref 26. Correlation functions in the depolarized DLS experi-

† This paper is dedicated to Professor Wilmer G. Miller on the occasion of his retirement.

* Corresponding author: e-mail paul.russo@chem.LSU.edu, phone (225) 578-5729; Fax (225) 578-3458.

10.1021/ma0205459 CCC: $22.00
Published on Web 10/01/2002

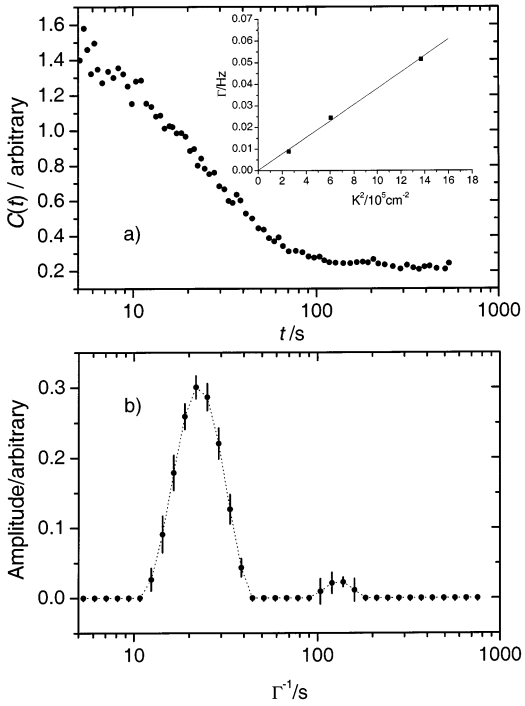

Figure 1. (a) Sample recovery profile for 1.0 mg/mL TMV. Inset: representative plot of the decay rate against the square of the spatial frequency; linear dependence indicates that the primary decay mode is diffusive. (b) CONTIN analysis of the same recovery profile. The weaker, slower mode was not present in all runs and did not scale well with the square of the spatial frequency.

ment suggested the TMV solution was nearly monodisperse. The sedimentation coefficient of $S_{20,w} = 190$S also confirmed the quality of the purified virus. The DLS translational diffusion coefficient of the labeled TMV, $D_{t,20w} = (4.8 \pm 0.08) \times 10^{-8}$ cm^2 s^{-1}, agreed with that of the unlabeled material, within error. This suggests that labeling does not damage the virus.

The labeled TMV behaved well in FPR experiments. There was sufficient signal despite the light labeling, and the samples were bleachable with pulses much shorter than the recovery time. Parasitic photobleaching during the recovery phase was minimal. One can account for this effect by analyzing the ratio of modulated (ac) signal to the steady (dc) signal, but no such corrections were necessary. Most recovery profiles exhibited two well-separated decay components as determined by two-exponential, nonlinear least-squares fitting and by the inverse Laplace transform program, CONTIN.[27,28] The larger, primary mode is clearly diffusive, as it scales with K^2 **(**Figure 1). The much weaker and slower decay mode did not scale with K^2 and was not present in all runs. A combination of low amplitude and correspondingly large decay rate uncertainties makes it difficult to assign physical significance to this mode. Possible causes include adhesion of TMV to the cell walls and, at higher concentration, nascent liquid crystalline droplets. A weak, fast-decaying component was sometimes evident, probably due to free dye or protein subunits not attached to the virus particle; the corresponding channels at short times were not included in the CONTIN fits. The analysis below relies on the primary decay mode, using the chosen solution found by CONTIN.

The dependence of D_{self} on TMV concentration appears in Figure 2, which spans the experimentally

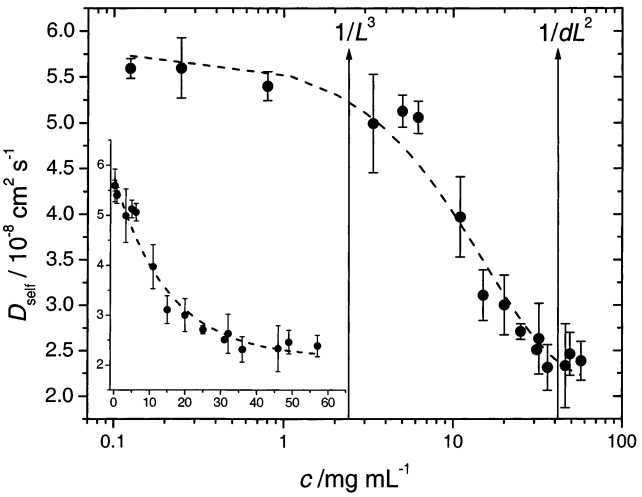

Figure 2. Measured self-diffusion coefficient plotted against concentration. The arrows define the semidilute regime for TMV of length $L = 3000$ Å and diameter $d = 180$ Å. The error in measured diffusion coefficients comes from linear fits of Γ vs K^2. The inset shows the same data using a linear scale for the concentration.

accessible portion of the isotropic regime. Lower concentrations would be difficult to measure, because of weak signal. More concentrated samples gave signs of incipient liquid crystal formation. (Some regions appeared birefringent when observed through crossed polarizers in a light microscope.) The value of D_{self} at the lowest concentrations agrees with the DLS result when corrected for temperature and viscosity. With concentration plotted logarithmically, the diffusion coefficient appears to be a nearly level function of concentration below $\nu \cong 1/L^3$, which corresponds to 2.45 mg/mL for the 3000 Å long TMV. At $\nu \cong 2.5/L^3$, a downturn in D_{self} seems apparent. Ultimately, D_{self} reaches about one-half its value in the dilute regime, as expected by Doi and Edwards for a rod that loses lateral mobility without a large effect on longitudinal motion. As only two points lie slightly above the curve in Figure 2, which represents a simple exponential fit, it is difficult to make a compelling case for any sudden transition.

The diffusion behavior of TMV differs from that of PBLG, as shown in Figure 3. While all the TMV solutions were at <6%, PBLG was measured at concentrations of up to 30%, depending on molecular weight. Such concentrations result in reduced solvent mobility; as discussed in ref 3, the best scaling of data for different PBLG molecular weights is achieved by factoring out the relative solvent diffusivity, $(D/D_0)_{solvent}$. Data for *N*,*N*′-dimethylformamide (DMF) were used to estimate the behavior of the solvent used for the PBLG measurements, which was pyridine. Solvent scaling is not responsible for the low-concentration plateau; it can be seen in plots without the solvent scaling (not shown, but see Figure 6 of ref 3 for an example). Compared to TMV, reductions in PBLG diffusion begin at much higher number densities, approximately $1/dL^2$. While delayed until concentrations much higher than $1/L^3$, the decrease in diffusion is ultimately more significant for PBLG than for TMV. At the highest concentrations supporting an isotropic phase, PBLG diffusion loses about 90% of its dilute solution mobility. TMV more closely approximates the expected behavior for rods:[11,12] loss of translational mobility is limited to a little more than 50%.

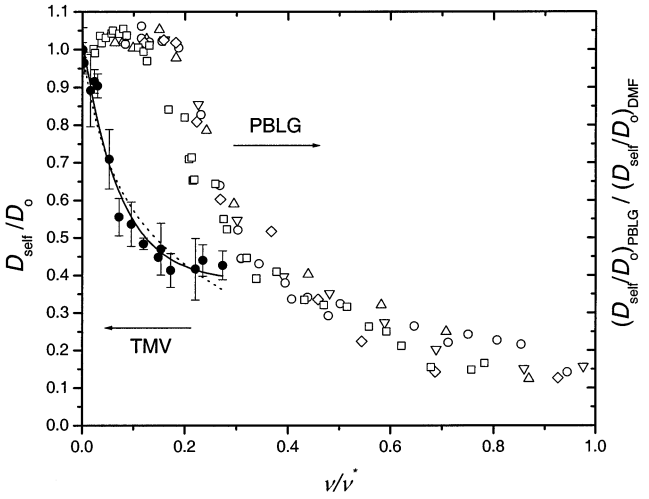

Figure 3. Solid points: TMV diffusion data normalized by zero concentration value. Curves: fit using eq 3 (dotted) and eq 4 (solid). Open points: labeled PBLG data from ref 3, normalized not only by the zero concentration value but also by a term reflecting solvent mobility (see text). Symbols represent different molecular weights: □, 20 000; ○, 36 000; △, 89 000; ▽, 103 000; ◇, 232 000. Reference 3 contains additional data for labeled PBLG at higher concentrations.

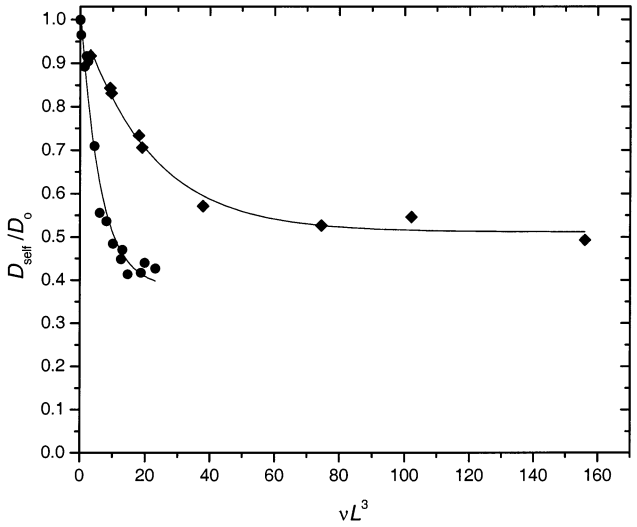

Figure 4. Simulations of Doi, Yamamoto, and Kano (◆) compared to results for TMV (●). Exponential decay fits are drawn through both data sets.

The most obvious explanation for the delayed onset of mobility-restricting interactions in PBLG is flexibility. A recent attempt[29] by this laboratory to estimate the persistence length of PBLG met with limited success because the polymer is not available at molecular weights high enough to display much flexure. Even with chromatographic separation and on-line light scattering detection, we could only suggest that values on the high side of the very wide published range were probably correct; i.e., the persistence length of PBLG may exceed 2000 Å. Some of the PBLG samples studied in ref 3 were much shorter than any reasonable estimate of the persistence length, so they might have been expected to behave like rigid rods. Perhaps the slightest flexure is sufficient to help rods evade constraints to their motion. An alternative and very speculative explanation for PBLG's behavior concerns helix stability, especially near the ends. Floppy ends might help an otherwise rigid polymer avoid entanglements at low concentrations, even as they raise the effective cross-section for longitudinal motion, causing extra hindrance at high concentrations.

The main result of this paper is that TMV self-diffusion decreases by about half, and almost exponentially, as the concentration is raised in the isotropic regime. Evidence for any sudden onset of mobility reduction is weak. Several theories have considered mechanistic details. Comparisons to these revealed little. The scaling approach of Tinland, Maret, and Rinaudo,[9] intended for wormlike chains, predicts the observed level and then falling behavior of D_{self} on a log−log scale, though with a much stronger concentration dependence in the strongly decreasing regime. The Edwards and Evans[18] based theoretical approach of Teraoka and Hayakawa[14] for perpendicular diffusion of thin rods and that of Sato and Teramoto[13] for parallel diffusion were combined in ref 3 to yield expressions for the average diffusion coefficient. An example is

$$D/D_0 = \frac{1}{2}[(1 - \delta v/v^*)^2 + (1 + \psi v/v^*)^{-2}] \qquad (3)$$

where $\delta = 16\alpha/\pi$ and $\psi = \epsilon\nu^* L^3$ (α and ϵ are unitless constants). A not entirely satisfying fit of this equation to the data (Figure 3) yielded values of $\delta = 0.75 \pm 0.28$ and $\psi = 8.5 \pm 1.7$, which are fairly close to some values for PBLG.[3] Lack of variable length TMV particles precludes examination of the expected scaling of ψ with length. The variational approach of Dhont, van Bruggen, and Briels[17] treats the first-order concentration dependence of the long-time self-diffusion coefficient for rods of finite aspect ratio (i.e., $D_{self}/D_0 = 1 - \alpha'\psi +$ higher terms). Using their eq 33 for α', a function of the aspect ratio, and the known dimensions of TMV predicts $\alpha' \approx 11.5$. A fit to the dilute regime TMV data yields a value about twice as large.

If the data fail to match any of the detailed mechanistic theories, they do at least exhibit a simple phenomenology. The available data can be fit to an exponential decay in any of several common concentration scales:

$$D_{self}/D_0 = b + ae^{-k'x} \qquad (4)$$

where $b = 0.38 \pm 0.03$, $a = 0.64 \pm 0.03$, and k' can be expressed for the various concentration (x) scales as follows: for mass density ($x = c$), $k' = 66 \pm 10$ mL g^{-1}; for number density ($x = \nu$), $k' = (4.4 \pm 0.66) \times 10^{-15}$ mL; for number density reduced to the Onsager critical density ($x = \nu/\nu^*$), $k' = 14 \pm 2$; for number density reduced to dL^2 ($x = \nu dL^2$), $k' = 2.7 \pm 0.4$; and for number density reduced to L^3 ($x = \nu L^3$), $k' = 0.16 \pm 0.02$. Exponential declines in diffusivity have been observed in many probe diffusion studies not involving rods.[36,37]

Comparison to the available simulations[30−35] provides another frame of reference. Brownian dynamics simulations by Bitsanis, Davis, and Tirrell[35] find that the center-of-mass diffusivity decreases to slightly less than half its value at zero concentration, as observed here. The Brownian dynamics simulations for infinitely thin rods by Doi, Yamamoto, and Kano[30] suggest a center-of-mass diffusion coefficient that smoothly decreases with concentration to a predetermined $0.5D_o$. In Figure 3 of ref 30, the authors chose a logarithmic scale for their concentration axis, and the shape resembles our Figure 2. Their simulation results appear on a linear scale alongside our TMV data in Figure 4. A very

satisfying exponential fit to the simulation data gives $D/D_0 \sim 0.5 + \exp(-\nu L^3/21)$. That is, $k' = 0.047$ (number densities scaled to L^3) for thin rods by the Brownian dynamics simulation of ref 30. TMV diffusion decreases with concentration about 3 times faster ($k' = 0.16$). Possible causes include the finite thickness of the TMV, hydrodynamic interactions ignored by the simulations, and aggregation at the higher concentrations.

While it is impossible to rule out aggregation, the wholesale variety that would produce large, stable particles would have consistently produced large-amplitude, slow decay modes to confound the CONTIN analysis. Instead, the occasionally observed slow decay modes were usually weak and easily isolated from the main decay. Limited side-by-side aggregation would have only a minor effect, but end-to-end assembly is potentially more troublesome. The present results could be explained by postulating that TMV assembles lengthwise into stable particles with an average aggregation number of two, without experiencing any topological constraints. It seems far more likely that aggregation of any type is limited, that topological constraints act to reduce the diffusion coefficient by about the expected amount, and that finite thickness and hydrodynamic interaction conspire to make the decrease more rapid and slightly more significant than in the simulations.

Conclusion. It is not possible to make a compelling case that translational diffusion in TMV exhibits any sudden reduction to signal the onset of enmeshment. Interactions occur at lower concentrations than they did in PBLG and are surely effective by $\nu \sim 2.5/L^3$. About 60% of the diffusion is lost before the liquid crystalline transition occurs, very close to the 50% expected by the Doi−Edwards theory for long, thin rods. The high axial ratio, stiffness, and monodispersity of TMV make it a useful system for testing theories of rods. Drawbacks include thickness and the inability to vary length. It remains to explain how PBLG successfully evades enmeshment until the number density reaches about $1/dL^2$, independent of total length. The overall reductions are also larger for PBLG than for TMV, suggesting the importance of flexibility, helix instabilities near the ends, or both.

Acknowledgment. We acknowledge Jonathan Strange for growing, infecting, and harvesting the tobacco plants. This work was supported by National Science Foundation Award DMR-0075810 and a Louisiana Board of Regents Fellowship to R.C.C., who thanks Dr. Nancy Thompson for her hospitality and the use of the Innova 90 laser source during his extended stay at the University of North Carolina−Chapel Hill.

References and Notes

(1) de Gennes, P.-G. *Scaling Concepts in Polymer Physics*; Cornell University: Ithaca, NY, 1979.
(2) Lodge, T. P.; Muthukumar, M. *J. Phys. Chem.* **1996**, *100*, 13275−13292.
(3) Bu, Z.; Tipton, D. L.; Negulescu, I. I.; Russo, P. S. *Macromolecules* **1994**, *27*, 6871−6882.
(4) van Bruggen, M. P. B.; Lekkerkerker, H. N. W.; Maret, G.; Dhont, J. K. G. *Phys. Rev. E* **1998**, *58*, 7668−7677.
(5) van Bruggen, M. P. B.; Lekkerkerker, H. N. W.; Dhont, J. K. G. *Phys. Rev. E* **1997**, *56*, 4394−4403.
(6) Scalettar, B. A.; Hearst, J. E.; Klein, M. P. *Macromolecules* **1989**, *22*, 4550−4559.
(7) Wang, L.; Garner, M. M.; Yu, H. *Macromolecules* **1991**, *24*, 2368−2376.
(8) Seils, J.; Pecora, R. *Macromolecules* **1995**, *28*, 661−673.
(9) Tinland, B.; Maret, G.; Rinaudo, M. *Macromolecules* **1990**, *23*, 596−602.
(10) Zero, K. M.; Pecora, R. *Macromolecules* **1982**, *15*, 87−93.
(11) Doi, M.; Edwards, S. F. *J. Chem. Soc., Faraday Trans. 2* **1978**, *74*, 560−570.
(12) Doi, M.; Edwards, S. F. *J. Chem. Soc., Faraday Trans. 2* **1977**, *74*, 918−932.
(13) Sato, T.; Teramoto, A. *Macromolecules* **1991**, *24*, 193.
(14) Teraoka, I.; Hayakawa, R. *J. Chem. Phys.* **1988**, *89*, 6989.
(15) Szamel, G. *Phys. Rev. Lett.* **1993**, *70*, 3744.
(16) Semenov, A. N. *J. Chem. Soc., Faraday Trans. 2* **1986**, *82*, 317−329.
(17) Dhont, J. K. G.; van Bruggen, M. P. B.; Briels, W. J. *Macromolecules* **1999**, *32*, 3809−3816.
(18) Edwards, S. F.; Evans, K. E. *J. Chem. Soc., Faraday Trans. 2* **1982**, *78*, 113−121.
(19) Kirchhoff, Th.; Lowen, H.; Klein, R. *Phys. Rev. E* **1996**, *53*, 5011−5022.
(20) Odijk, T. *Macromolecules* **1986**, *19*, 2073−2074.
(21) Onsager, L. *Ann. N.Y. Acad. Sci.* **1949**, *51*, 627.
(22) Cush, R.; Russo, P. S.; Kucukyavuz, Z.; Bu, Z.; Neau, D.; Shih, D.; Kucukyavuz, S.; Ricks, H. *Macromolecules* **1997**, *30*, 4920−4926.
(23) Haugland, R. P. *Handbook of Fluorescent Probes and Research Chemicals*; Molecular Probes: Eugene, OR, 1996.
(24) Fong, B.; Stryjewski, W.; Russo, P. S. *J. Colloid Interface Sci.* **2001**, *239*, 374−379.
(25) Lanni, F.; Ware, B. R. *Rev. Sci. Instrum.* **1982**, *53*, 905.
(26) Wilcoxon, J.; Schurr, J. M. *Biopolymers* **1983**, *22*, 849−867.
(27) Provencher, S. W. *Comput. Phys.* **1982**, *27*, 213−227.
(28) Provencher, S. W. *Comput. Phys.* **1982**, *27*, 229−242.
(29) Temyanko, E.; Russo, P. S.; Ricks, H. *Macromolecules* **2001**, *34*, 582−586.
(30) Doi, M.; Yamamoto, I.; Kano, F. *J. Phys. Soc. Jpn.* **1984**, *53*, 3000−3003.
(31) Fixman, M. *Phys. Rev. Lett.* **1985**, *54*, 337−339.
(32) Frenkel, D.; Maguire, J. F. *Mol. Phys.* **1983**, *49*, 503−541.
(33) Keep, G. T.; Pecora, R. *Macromolecules* **1985**, *18*, 1167−1173.
(34) Lowen, H. *Phys. Rev. E* **1994**, *50*, 1232−1242.
(35) Bitsanis, I.; Davis, H. T.; Tirrell, M. *Macromolecules* **1990**, *23*, 1157−1165.
(36) Phillies, G. D. J. *J. Phys. Chem.* **1989**, *93*, 5029−5039.
(37) Phillies, G. D. J. *Macromolecules* **1986**, *19*, 2367−2376.

MA0205459